HHS Public Access

Author manuscript

Magn Reson Med. Author manuscript; available in PMC 2019 April 01.

Published in final edited form as:

Magn Reson Med. 2018 April ; 79(4): 1931–1940. doi:10.1002/mrm.26845.

Evaluation of spiral acquisition variants for functional imaging of human superior colliculus at 3T field strength

Vimal Singh[1], **David Ress**[2,*], **Josef Pfeuffer**[3], and **Tiejun Zhao**[4]

[1]Electrical and Computer Engineering Department, The University of Texas at Austin, Austin, TX, USA

[2]Department of Neuroscience, Baylor College of Medicine, Houston, TX, USA

[3]Siemens Healthcare, Application Development, Erlangen, Germany

[4]Siemens Healthcare, MR Research Collaborations, Pittsburgh, PA, USA

Abstract

Purpose—High-resolution functional magnetic resonance imaging of human subcortical brain structures is challenging because of their deep location in the cranium, and their comparatively weak BOLD responses to strong stimuli. Magnetic resonance imaging data for subcortical brain regions exhibit both low signal-to-noise ratio and low functional contrast-to-noise ratio (CNR). To overcome these challenges, this work evaluates the use of dual-echo spiral variants that combine outward and inward trajectories. Specifically, in-in, in-out, and out-out combinations are evaluated. For completeness, single-echo spiral-in and parallel-receive-accelerated echo-planar-imaging sequences are also evaluated.

Methods—Sequence evaluation was based on comparison of functional contrast-to-noise ratio within retinotopically predefined regions of interest. Superior colliculus (SC) was chosen as sample subcortical brain region because it exhibits a strong visual response. All sequences were compared relative to a single-echo spiral-out trajectory to establish a within-session reference.

Results—In SC, the dual-echo out-out outperformed the reference trajectory by 55% in CNR, while all other trajectories had performance similar to the reference. The sequences were also compared in early visual cortex. Here, both dual-echo spiral out-out and in-out outperformed the reference by ~25%.

Conclusion—Dual-echo spiral variants offer improved CNR performance for high-resolution imaging for both SC and cortex.

Keywords

MRI; fMRI; pulse sequence; spiral; signal-to-noise ratio; contrast-to-noise ratio

[*]Corresponding author: David Ress, Department of Neuroscience, Baylor College of Medicine, One Baylor Plaza, Suite S104, Houston, TX-77030, USA, ress@bcm.edu.

Introduction

Human brainstem mediates a panoply of critical brain functions that range from homeostasis to cognition. It is, therefore, desirable to develop effective functional magnetic resonance imaging (fMRI) methods for brainstem. A model brainstem nucleus of particular interest is superior colliculus (SC), a laminar structure, with three millimeter-scale laminar subdivisions: superficial layers that receive direct retinal inputs, intermediate layers associated with visual attention and oculomotor responses, and deep layers that play a role in multi-sensory integration (1). The superficial visual layers contain a retinotopic representation of visual space (2–5), and thus are an ideal subject to study high-resolution brainstem imaging because their organization permits delineation of small retinotopically specific regions of interest (ROIs).

To our knowledge, the highest spatial resolution (1.2-mm isometric voxels) at 3T field strength has been obtained using multi-shot spiral acquisition. These methods have successfully delineated visual field maps in the superficial layers of SC (6), measured depth profiles of sub-cortical activity in retinotopically delineated ROIs in SC (3), and resolved depth profiles of sound frequency selectivity in inferior colliculus (7). The success of this work motivated this study to further evaluate spiral acquisition methods for sub-cortical brain regions.

Functional imaging in brainstem is challenging compared to cerebral cortex for two main reasons. First, small voxels are essential to resolve sub-cortical nuclei, which are small (typically < 1 cm) in size and densely packed. The necessary spatial resolution compromises slice coverage. Thus, fMRI studies in brainstem are similar to neurophysiology, in that a small brain region is studied in careful detail, rather than imaging the whole brain. Second, signal levels are lower while noise levels are higher than in cortex. Signals are reduced in brainstem nuclei mostly because of their deep location. Functional contrast levels are also relatively low, even for the strongest visual stimuli. At the same time, noise levels can be higher in brainstem subcortical nuclei because they are adjacent to large vascular structures that supply and drain blood from the brain. Therefore, physiological nuisance artifacts are particularly pronounced in superficial brainstem structures such as SC. Thus, SC offers the challenge of obtaining high spatial resolution despite particularly low CNR.

Echo Planar Imaging (EPI) and spiral are the two most commonly used trajectories for fMRI acquisitions. An EPI trajectory covers *k*-space in a raster fashion, and in doing so it uses the underlying gradient systems inefficiently. The need for continual polarity reversals in gradient amplitude generally does not permit operation at full power; instead the trajectories are slew-rate limited (8). Spiral trajectories use the gradient system more efficiently through equal energy deposition in two gradient directions, and by avoiding sharp corners in the k-space trajectory (8–10). Spiral trajectories therefore have relatively shorter readout durations than similar EPI trajectories. However, independent of the trajectory, to obtain high-resolution fMRI with satisfactory SNR requires long readout durations compared to the T_2^* signal decay in gray matter. For this reason, multi-shot acquisitions are necessary; however, they are susceptible to motional inter-shot off-resonance errors. Multi-shot spiral acquisition is amenable to self-navigation schemes, reducing some of the shot-to-shot errors. Also, the

trajectory oversamples low spatial frequencies, which renders head motion as blurring in recovered images as opposed to ghosting in EPI, thereby making spiral acquisitions relatively more robust to motion than the EPI (8, 10).

Most fMRI studies in SC have used EPI. An early study found lateralization of the visual responses between the two SC (11) using 1.56×1.56×3-mm voxels. More recently, Schneider & colleagues (5, 12) delineated visual field mappings in SC with 1.5×1.5×2-mm voxels. However, it is often clear in these studies that additional spatial resolution would be useful. Much recent fMRI work in cortex has also made use of symmetric multi-slice (SMS) methods (13, 14). Such approaches are very attractive because they increase slice coverage with little signal-to-noise ratio (SNR) loss, although imperfections in the slice unaliasing process can also lead to artifacts and functional mislocalization. SMS methods could also be utilized in brainstem but, because both SNR are so limited in these brain regions, and because coil-element sensitivities are so uniform, SMS may be less effective for these applications.

The spiral trajectory is asymmetric with respect to the echo time, and the most commonly used variant starts at the origin and moves outwards, which we will term spiral *out*. The variant that starts from *k*-space periphery and moves inwards will be termed spiral *in*. Spiral in improves upon the TR efficiency of spiral out, while acquiring a comparably similar T_2^*-weighted image (15). In addition, spiral in exhibits lower signal dropout than spiral out for regions compromised by macroscopic susceptibility field gradients (SFGs) near the air-tissue interfaces (16, 17). However, in homogeneous regions, spiral in shows lower sensitivity to Blood Oxygen Level Dependent (BOLD) contrast than the out variant (17, 18). Spiral variants also include dual-echo trajectories that traverse *k*-space twice after each excitation. The in-out variant is the most widely studied and was previously shown to reduce signal loss in regions compromised by SFGs and increase image SNR in homogeneous regions resulting in increased BOLD activation volumes (16–18). More recently, the in-in variant was found to be superior to in-out variant in terms of recovering BOLD activation in regions affected by SFGs(19). In the same study, the out-out variant was shown to yield images with the highest image SNR among dual-echo variants (19).

Here, we evaluate the use of dual-echo spiral variants for high-resolution sub-cortical fMRI. Acquisition of two echoes should increase the available contrast to improve BOLD sensitivity of high-resolution fMRI. Due to an inadequate knowledge of fMRI noise processes at high resolutions, it is difficult to extrapolate the results of previous low-resolution studies to the high-resolution regime. Moreover, previous studies focused on signal recovery in regions affected by SFGs, and therefore measured BOLD sensitivity using activation volumes. This measure is not satisfactory to assess the performance of high-resolution imaging applications.

Similar to previous studies, image SNR values are calculated and reported, extending their results to a high-resolution regime. Moreover, unlike previous studies, BOLD sensitivity is characterized through activation signal and noise amplitudes within functionally and anatomically defined ROIs. The separate consideration of contrast and noise enable a more detailed evaluation of sequence performance and the challenges of sub-cortical imaging. For

reference, BOLD sensitivity is also evaluated in early visual cortex (EVC), which has been extensively studied and well characterized in the past. Because spiral sequences have limited availability, we also present results acquired using an EPI approach that can also provide useful results in SC.

Methods

MRI

Imaging was performed on 3T scanners (Skyra and Trio, Siemens Healthcare, Erlangen, Germany) using the product 32-channel head coil and a research spiral imaging sequence. Fig. 1a shows an example prescription and a functional image from a single-echo spiral-out acquisition. In this prescription, twelve 1.2-mm-thick quasi-axial slices were oriented roughly perpendicular to the local neuraxis to cover the entire SC with a 192-mm field-of-view (FOV). This prescription also samples a portion of early visual cortex.

For five spiral sequence variants (out, in, in-in, in-out and out-out), we chose TR = 1 sec, so with three interleaves, a volume was acquired every 3 seconds. Uniform spiral trajectories were generated using standard methods; see Supporting Material. Gradient strength of 24 mT/m and a slew rate of 150 T/m/s resulted in T_{acq} = 35 ms at bandwidth 200 kHz. For all dual-echo spiral variants, the two acquisitions were concatenated without delay, so that $TE_2 = TE_1 + T_{acq} + T_{refocus}$ for the out-out and in-in variants and, $TE_2 = TE_1$ for in-out variant, where $T_{refocus} \ll 1$ ms. Pulse sequence waveforms for spiral variants are shown in Fig. S1. For dual-echo variants, we used the first-echo TE as a tuning parameter.

In analogy, we used 3x GRAPPA acceleration to obtain the same resolution using the product EPI sequence (20–22) with a 154-mm FOV, echo spacing of 1.30 ms, and T_{acq} = 49 ms. To avoid fold-over effects, a 100-mm-wide saturation band was prescribed over the anterior portion of the head (23). The resulting set of images was temporally rebinned to 3-sec sampling to improve SNR and allow comparison with the spiral data.

A set of T1-weighted structural images was obtained on a prescription co-aligned with the above structural images at the end of each scan session using a 3D FLASH sequence (15° flip angle, 0.78-mm pixels, minimum TE and TR). These images were used to align the functional data to the segmented structural reference volume (see below).

Further details are provided in the Supporting Information.

Structural imaging

In a separate session for each subject, we acquired a structural reference volume with good gray-white contrast using a MP-RAGE sequence (TI = 950 ms, 9° flip angle, isometric voxel size of 0.7 mm, two averages, 25-min duration). The anatomical images collected in each functional scan session were used to align the functional data to this structural 3D reference volume. Fig. 1b shows a structural axial slice (1st row-left) and the corresponding transformed functional data acquired using spiral-out, spiral-in and EPI trajectories (2nd–4th row-left). The image projections in the transformed functional data correspond to the overlap between the structural volume and anatomical slice prescription. Because the different

trajectories were acquired in different sessions with different slice prescriptions, these image volume projections vary somewhat. The insets (in fig. 1b-right) show enlargements from the structural and functional data; yellow lines show boundaries of SC tissue evident in the T1-weighted image and at corresponding locations contrast boundaries are also visible in the functional images. The results confirm the effective spatial registration of the spiral and EPI acquisitions.

From the structural volume, we segmented the tissue of the midbrain, brainstem, and portions of the thalamus using a combination of automated and manual methods provided by the ITK-SNAP application (24). The CSF-tissue interface of the brainstem is interpolated from the segmentation using isodensity surface tesselation, and this initial surface was refined to reduce aliasing artifacts using a volume-preserving deformable-surface algorithm (Fig. 2b) (25). In cortex, the FreeSurfer software suite was used to initially segment the white matter and gray matter at 1-mm sampling (26). These segmentations were then upsampled to 0.7-mm and adjusted manually to correct errors and obtain full resolution (27). At the adjusted gray-white interface, a smooth surface was obtained using the same methods used for brainstem.

Image analysis

An alternating lateralized hemifield stimulation with a demanding task was used to evoke a strong functional response in SC and visual cortex (Fig. 1c) while fMRI data were collected. Data were corrected for motion and slow drifts, and intensity normalized. A sinusoid at the stimulus repetition frequency was then fit to the normalized time series at each voxel, and from this fit we derived volume maps of response amplitude, coherence, and phase. The amplitude quantifies the functional contrast (Fig. 2). To quantify BOLD noise, bootstrapping (28–30) across sessions was used to estimate the contrast statistical distribution. BOLD noise amplitude was defined as half the difference between the upper and lower 68% confidence intervals of this distribution as shown in Fig. S3. Data from the several runs for each trajectory were then averaged together to improve CNR, and averaged through the superficial layers of SC. Retinotopic ROIs (Fig 2) were obtained for each subject from the initial reference sessions. The sinusoidal fitting procedure also provided a map of coherence (correlation with the best-fit sinusoid) upon each SC. We manually chose the point of maximum coherence upon rostral SC, which contains the retinotopic representation of the stimulus aperture, and expanded this region in a fashion that maximized the mean coherence of a contiguous region of SC with area 6–8 mm^2 around this point; this area was chosen based on the expected retinotopic distribution of the stimulus representation (4). SC ROIs delineated using this process for a subject are overlaid atop the coherence amplitude and phase maps in Figs. 2e & 2f, respectively. In visual cortex, we defined ROIs from the baseline session by choosing the top 50% of coherence within visual areas V1–3. Visual areas were defined for each subject in separate fMRI sessions using a tomographic PRF method (31). Fig. 2c–d shows the visual areas V1–3 in the left and right hemisphere, respectively. For details, see Supporting Material.

Data Acquisition

Tuning Data—We tuned each trajectory to find the optimal echo time at which it yielded the highest BOLD CNR. To tune each variant, functional data was acquired on a single subject over a broad range of echo times. Data was analyzed and CNR calculated in a selected ROI. A parabola was fit to the CNR for various echo times, and the peak of the parabola estimated the optimal TE. For each variant, a subject was selected from a pool of three healthy volunteers. For each echo time, 6 functional runs of ~4 min. duration each were acquired. Data acquisition for all echo times for a variant are distributed over two acquisition sessions with 2–3 different echo times per session. This resulted in tuning sessions of 12–18 functional runs.

Comparison Data—Functional data was acquired on five healthy volunteers (age 25–55 years, mean 35 ± 12 years; one female) for spiral variants: in, in-in, in-out and out-out, and for EPI. Single-echo spiral-out was used as a reference trajectory. In each comparison session, seven runs each were acquired for spiral-out and for one of the five aforementioned trajectories. To account for day-to-day variability, two comparison session were acquired per subject per trajectory. Thus, a total of 10 comparison sessions were acquired per trajectory.

Results

Previous studies used image SNR as a metric for comparing the performance of the sequence variants. To establish a point of comparison of our results to these studies, we measured SNR for each of our dual-echo trajectories. Fig. 3 compares SNR values obtained in EVC and SC in our studies to those obtained by a previous study (19). Li and colleagues had 12 healthy volunteers perform a complex finger tapping task while whole-brain fMRI data were acquired on a 1.5T scanner using 3.8-mm isometric voxels for a ROI defined in motor cortex; imaging data was acquired for in-in and out-out spiral variants. The in-out data was then constructed using the first and second echoes from in-in and out-out variants, respectively. In comparison, our results are acquired using 1.2-mm isometric voxels on a 3T scanner by direct acquisition of all three variants.

A comparison of relative trends extends the results of the previous study into a high-resolution regime. The effects of high resolution are clearly evident. For the single echoes, SNR was about two-fold lower in cortex at high resolution, and drops by another factor of two in SC. When the two echo images are directly averaged, for both low and high resolution, SNR increases in the order: in-in, in-out and out-out in cortex. However, there is no longer a significant difference between the in-in and in-out pairs. In SC, there is again no difference in SNR between in-in and in-out, but out-out is clearly stronger.

Temporal SNR values for EPI and the single-echo spiral reference were obtained across the many sessions. In EVC, we observe mean SNRs of 27.3±5.3 for EPI as compared to 36.9±5.3 for the reference. In SC, we observe 11.3±1.4 for EPI as compared to 19.1±2.5 for the reference. Thus, EPI appears to provide a significantly lower temporal SNR than the single-echo spiral reference trajectory ($P < 0.0004$).

CNR varies somewhat with echo time for the various trajectories. Parabolic fits to CNR versus echo time were used to estimate optimal echo time for each trajectory. Fig. 4 shows the data and the fits in EVC; optimal echo times from the fits are marked on the plots. The data in SC were of poorer quality than EVC due to much lower CNR. However, since the T_2^* is similar in both SC and EVC ROIs and the broad-peak fits obtained in EVC indicate weak sensitivity of CNR to TE, we chose to use optimal echo times from EVC. For dual-echo spiral variants we used the Sig-wt combined data for the fits and used the echo-time of first echo for reference. The fitting process is effective for most of the variants, but spiral out-out did not exhibit a clear maximum; CNR was not much affected by TE.

Figs. 5a & b show mean contrast and noise for dual-echo spiral variants in EVC and SC, respectively. Data is shown for the individual echoes, the combined echoes and the single-echo spiral-out reference acquisition for comparison. In EVC, all dual-echo variants show higher contrast for the second echo than the first. In SC, the same pattern is evident for spiral out-out, but the first echo is stronger than the second echo for both in-in and in-out. For all variants, the second echo is noisier than the first echo.

Contrast and noise are affected differently when the individual echoes are combined by the three methods. For the signal-weighted (Sig-wt) combination, contrast and noise roughly follow the echo that exhibits the higher mean image intensity. This is clearest for the in-in and out-out variants, for which the first echo has a mean intensity that is stronger than the second echo by a factor of $e^{\frac{T_{acq}}{T_2^*}}$ For the contrast-weighted (CTNR-wt) combination, it is difficult to interpret its effect because of its more complex combination-weight calculation. For the contrast-sum (C-sum) approach, the contrast sum results in a large increase in contrast, but also a substantial increase in noise. The CNR difference between EVC and SC is dramatic: CNR in EVC is 9.2× larger than in SC. The combination schemes offer differing performance improvements over the individual echoes. The Sig-wt and CTNR-wt schemes consistently perform better than the C-sum scheme. Comparatively, for both Sig-wt and CTNR-wt schemes, a reduction in BOLD noise is observed that leads to an increase in CNR over the individual echoes.

Figs. 5c & d show CNR normalized to the reference acquisition. Error bars reflect the standard-error-of-the-mean (SEM) across sessions. The Sig-wt and CTNR-wt combination schemes generally succeed in increasing CNR over the individual echoes, but performance is mixed for the C-sum scheme. Overall, there are no significant differences between the combination schemes. There are weak trends for the Sig-wt and CTNR-wt schemes to outperform the C-sum scheme ($P \sim 0.3$). Generally, the Sig-wt and CTNR-wt schemes perform about the same. We therefore chose to use the Sig-wt scheme in further analysis because it is blind to the experiment design.

Fig. 6a shows contrast and noise normalized to the reference trajectory for each of the five trajectory variants in EVC. EPI performance is similar to the reference spiral out. Interestingly, spiral in offers a trend toward contrast improvement ($P = 0.11$), while noise remains largely unchanged. When two spiral in echoes are combined, however, the contrast improvement is smaller, but noise increases substantially. The spiral in-out combination

produces significantly greater contrast ($P < 0.002$), with a variable increase in noise ($P \sim 0.26$). Finally the out-out combination produces lower contrast ($P \sim 0$), but even lower noise ($P < 0.01$).

Fig. 6b shows normalized contrast and noise for the five trajectory variants in SC. For most of the trajectory variants, the large errors are indicative of the small CNR observed in SC. All trajectories except the out-out show improvement in contrast over the reference, although there is also an increase in noise. The increase in contrast is non-significant: EPI, $P \sim 0.12$; spiral in, $P \sim 0.19$; in-in, $P \sim 0.11$, and in-out, $P \sim 0.14$. In comparison, the increase in noise is significant: EPI, $P < 0.006$; spiral in, $P < 0.008$; in-in, $P < 0.02$; and in-out, $P < 0.03$. The out-out variant shows a trend for lower contrast ($P \sim 0.21$), but produces significantly less noise ($P < 0.005$).

Fig. 6c shows the mean relative CNR for the five trajectories in EVC. There are trends for improved CNR for three of the variants. Single-echo spiral in is marginally superior to the reference (mean improvement 13%, $P = 0.11$). Greater improvements are seen for spiral in-out (mean 27%, $P = 0.06$), and spiral out-out (mean 24%, $P = 0.07$). EPI performance is similar to the reference acquisition, and spiral in-in is slightly worse.

In SC (Fig. 6d), only the dual-echo spiral out-out shows better performance than the reference acquisition (mean 55%, $P = 0.05$). Performance of the other variants is statistically indistinguishable from the reference.

The various trajectories sample *k*-space differently, so we calculated the PSF for spiral in, spiral out, and EPI (Fig. 7) including transverse decay (top row) and in the fast-acquisition limit (middle row). Spiral in yields the narrowest PSF, 1.24 mm, which is only very slightly narrowed by transverse decay effects. By contrast, the spiral out PSF FWHM is 1.65 mm, 33% broader in size, and reflecting a 77% larger pixel volume. T_2^* decay produces some blurring, increasing the FWHM by about 9%. Finally, the EPI PSF is distinctly broader and non-circular in comparison to the spiral PSFs. The EPI PSF has a “plus-sign” shape, consistent with its rectilinear traversal of *k*-space. This distortion broadens the PSF to 1.86 mm. Compared to spiral out, the EPI PSF is about 13% larger in diameter, a 27% volumetric increase. Transverse decay has very little effect on the EPI PSF.

Discussion

Our results quantify signal, contrast, and noise for high-resolution fMRI in both early visual cortex (EVC) and superior colliculus (SC). Results dramatically illustrate the challenges of subcortical imaging because of its lower SNR and much lower CNR. The low-resolution data in Fig. 3 cannot be directly compared to the current high-resolution data because of differences in field strength, scanner vendor, etc., but we can make detailed comparison between the high-resolution data in EVC and SC. Overall, the drop in SNR is only a factor of two between the two areas, and this mostly reflects reduced signal because SC is located farther from the coil elements. The 9.2× CNR reduction of SC is mostly the consequence of reduced contrast (4.2×), with a milder noise increase (~2.2×). Thus, midbrain imaging is predominantly difficult because BOLD contrast here is much lower than that in cortex, but

increased noise also plays a role. Combining dual echoes is one strategy for dealing with the low CNR.

We used functional CNR as a metric to compare the performance of various multi-shot spiral variants for high-resolution imaging in human SC. A similar performance analysis was also applied to a GRAPPA-accelerated EPI acquisition. All acquisition trajectories were first evaluated to estimate optimal echo times. For each trajectory, optimal TE was chosen as the peak of parabola fitted to CNR values at multiple TEs for a subject. In SC, most spiral variants, and EPI, had similar performance. However, we observed significantly superior performance for the dual-echo spiral out-out variant. For comparison, we also evaluated CNR performance in EVC. Here we again found similar performance for both spiral-out and EPI acquisitions. Notably, both spiral in-out and out-out offered the best performance, about ~25% better than the reference. Single-echo spiral in also offered a small performance boost of ~13%.

Although EPI performed similarly to single-echo spiral out, it is notable that the acquisition time for the EPI trajectory was 49 ms as compared to 35 ms for the spiral. This longer acquisition time should increase raw SNR by 18%. There was, however, no evidence for this improvement in either SNR or CNR; SNR was significantly lower, while CNR was similar to the single-echo spiral-out reference trajectory. Thus, the efficient use of gradient systems by the spiral trajectory appears to provide a small improvement in performance over EPI. However, it proved feasible to overcome this decrement with a longer acquisition time. It is likely that the symmetry of the EPI acquisition permits longer acquisitions with less degradation from transverse signal decay than spiral.

Our sequence performance evaluation strategy focused specifically on CNR, which is a critical requirement for high-resolution fMRI studies. Previous studies (17, 19) focused on evaluating spiral variants for signal recovery in regions affected by susceptibility field gradients and evaluated performance using volume of activation above an arbitrary statistical threshold. Here, we used very small, ~10 μL, retinotopically specified ROIs in the superficial layers of SC, thus putting a premium on accurate spatial localization both within and across imaging sessions. Subcortical imaging experiments must focus on small functional units that deliver comparatively weak signals and contrast (2, 4, 5, 32) in the presence of strong physiological nuisance effects (33). Our results thus provide useful guidance in the selection of imaging schemes for such work.

The dual-echo spiral-out trajectory provided best performance in SC. The first echo delivers relatively less contrast, but with much lower noise than either the reference acquisition or the second echo. The second echo delivers much higher contrast, but the noise level is similarly increased. When the two echoes are then combined, the overall contrast is actually lower than the reference, but the noise is reduced still more. Apparently, this variant performs well because of noise suppression in the signal-weighted averaging process.

Both spiral out-out and in-out performed well in EVC. Spiral out-out again obtains its performance boost from noise suppression. Spiral in-out operates differently, offering a substantial increment in contrast with a relatively smaller increment in noise.

The performance of sequences using an inward spiral trajectory in SC was somewhat disappointing, because spiral in appears to offer greater temporal acquisition efficiency. It is possible that these trajectories were sensitive to small gradient errors during the initial pre-phase lobe. However, we observed similar fidelity between contrast boundaries for both spiral in and spiral out images, so trajectory fidelity was probably satisfactory. Also, sequences containing the spiral-in trajectory did show improvements in EVC. Certainly, the smaller ROIs in SC require finer spatial resolution than those in EVC. Each dual-echo combination provides different weightings of the spatial-frequency content within the BOLD contrast. Thus, it would appear that the dual-echo spiral out provides a better weighting for high spatial resolution. However, the SC data is considerably noisier than that in EVC, so it may be that finer details of trajectory performance will require more experimentation to improve statistical power.

We evaluated three schemes for combining the two echoes: signal-weighted, contrast-to-temporal-noise-ratio-weighted, and contrast-sum. There were no statistically significant differences between these schemes, but the contrast-sum scheme had a trend toward lower performance, while the other two schemes offered statistically similar performance. The signal-weighted scheme was therefore chosen because it is independent of the experiment design, which is consistent with previous results (16, 17).

Although the dual-echo variants performed better than the other schemes, the performance boost requires substantially higher total acquisition time. This increase in acquisition time can be compensated by reducing the volumetric coverage. For example, in our imaging protocols the spiral dual-echo out-out at TE = 30 ms can only acquire 9 slices in comparison to 12 slices for the reference single-echo out trajectory with TE = 40 ms. This 25% reduction in volumetric coverage is acceptable for studies focused on imaging small functional units such as the SC, but it is not satisfactory for imaging larger regions such as whole of early visual cortex. Otherwise, improving slice coverage would require increasing the repetition time, or reducing acquisition time through fewer interleaves or higher-speed trajectories at the cost of lower SNR. Altogether, the performance boost of multi-echo acquisition comes at a price of reduced volumetric coverage. Simultaneous multi-slice or multi-band methods (13, 14, 20–22) may offer a means to improve the volumetric coverage. However, the use of such methods in deep-brain regions such as SC, where SNR is low and coil sensitivity patterns are comparatively homogenous, has not yet been thoroughly explored. The PSF calculations cast additional light upon the performance differences between the sequences. Spiral out resolution is broadened by the filtering of transverse decay, resulting in an increase of ~24% in PSF volume. Thus, part of the improved CNR performance of the spiral-out variants can be attributed to degraded spatial resolution. The EPI PSF, by comparison, is broader than any of the spiral variants, because its non-circular sampling of *k*-space produces a “plus-sign” shape that is consistent with previous results (34). This distortion causes an area increase of 27% compared with spiral out, but this additional blurring does not appear to further improve CNR.

The asymmetry of EPI and the symmetry of spiral can be understood by considering the transforms of their corresponding *k*-space region-of-support (ROS) (Fig. 7, bottom row). Altogether, the PSF calculations indicate that dual-echo spiral out offers the best CNR

performance, but at a small cost in spatial resolution as compared to the variants that include spiral in.

Conclusions

High-resolution functional magnetic resonance imaging of human subcortical brain structures is challenging because of both low SNR and BOLD CNR. Here, we evaluated dual-echo spiral variants to improve the quality of BOLD contrast acquired from SC. Evaluation was based on comparison of BOLD contrast-to-noise ratio within retinotopically predefined regions of interest. In SC, dual-echo out-out offered significantly higher CNR performance than the other variants. In EVC, both dual-echo spiral out-out and in-out outperformed the others.

Supplementary Material

Refer to Web version on PubMed Central for supplementary material.

Acknowledgments

We wish to thank lab members Andrew Floren, Elizabeth Halfen, and Jung Hwan Kim for their tireless support as subjects in this project. Work supported by NSF BCS 1063774.

References

1. Wurtz RH, Albano JE. Visual-motor function of the primate superior colliculus. Annual review of neuroscience. 1980; 3:189–226.
2. DeSimone K, Viviano JD, Schneider KA. Population Receptive Field Estimation Reveals New Retinotopic Maps in Human Subcortex. The Journal of Neuroscience. 2015; 35:9836–9847. [PubMed: 26156986]
3. Katyal S, Ress D. Attentional base response in intermediate layers of human superior colliculus measured using high-resolution fMRI. Journal of Vision. 2013; 13:224.
4. Katyal S, Zughni S, Greene C, Ress D. Topography of Covert Visual Attention in Human Superior Colliculus. Journal of Neurophysiology. 2010; 104:3074–3083. [PubMed: 20861435]
5. Schneider KA, Kastner S. Effects of sustained spatial attention in the human lateral geniculate nucleus and superior colliculus. The Journal of Neuroscience. 2009; 29:1784–1795. [PubMed: 19211885]
6. Katyal S, Zughni S, Huk A, Ress D. Retinotopic maps of covert attention in human superior colliculus. Journal of Vision. 2009; 9
7. Ress D, Chandrasekaran B. Tonotopic Organization in the Depth of Human Inferior Colliculus. Frontiers in Human Neuroscience. 2013; 7:586. [PubMed: 24065909]
8. Glover GH. Spiral imaging in fMRI. NeuroImage. 2012; 62:706–712. [PubMed: 22036995]
9. Block KT, Frahm J. Spiral imaging: A critical appraisal. Journal of Magnetic Resonance Imaging. 2005; 21:657–668. [PubMed: 15906329]
10. Delattre BM, Heidemann RM, Crowe LA, Vallée JP, Hyacinthe JN. Spiral demystified. Magnetic Resonance Imaging. 2010; 28:862–881. [PubMed: 20409660]
11. DuBois RM, Cohen MS. Spatiotopic Organization in Human Superior Colliculus Observed with fMRI. NeuroImage. 2000; 12:63–70. [PubMed: 10875903]
12. Schneider K. Spatial and Feature-Based Attention in the Human Thalamus and Superior Colliculus. Canadian Journal of Experimental Psychology. 2012; 66:314–314.

13. Breuer FA, Blaimer M, Heidemann RM, Mueller MF, Griswold MA, Jakob PM. Controlled aliasing in parallel imaging results in higher acceleration (CAIPIRINHA) for multi-slice imaging. Magnetic Resonance in Medicine. 2005; 53:684–691. [PubMed: 15723404]
14. Setsompop K, Gagoski BA, Polimeni JR, Witzel T, Wedeen VJ, Wald LL. Blipped-controlled aliasing in parallel imaging for simultaneous multislice echo planar imaging with reduced g-factor penalty. Magnetic Resonance in Medicine. 2012; 67:1210–1224. [PubMed: 21858868]
15. Bornert P, Aldefeld B, Eggers H. Reversed spiral MR imaging. Magnetic Resonance in Medicine. 2000; 44:479–484. [PubMed: 10975902]
16. Glover GH, Law CS. Spiral-in/out BOLD fMRI for increased SNR and reduced susceptibility artifacts. Magnetic Resonance in Medicine. 2001; 46:515–522. [PubMed: 11550244]
17. Preston AR, Thomason ME, Ochsner KN, Cooper JC, Glover GH. Comparison of spiral-in/out and spiral-out BOLD fMRI at 1.5 and 3 T. NeuroImage. 2004; 21:291–301. [PubMed: 14741667]
18. Glover GH, Thomason ME. Improved combination of spiral-in/out images for BOLD fMRI. Magnetic Resonance in Medicine. 2004; 51:863–868. [PubMed: 15065263]
19. Li TQ, Takahashi A, Wang Y, Mathews V, Glover GH. Dual-echo spiral in/in acquisition method for reducing magnetic susceptibility artifacts in blood-oxygen-level-dependent functional magnetic resonance imaging. Magnetic Resonance in Medicine. 2006; 55:325–334. [PubMed: 16408267]
20. Feinberg DA, Moeller S, Smith SM, Auerbach E, Ramanna S, Gunther M, Glasser MF, Miller KL, Ugurbil K, Yacoub E. Multiplexed echo planar imaging for sub-second whole brain FMRI and fast diffusion imaging. PloS one. 2010; 5:e15710. [PubMed: 21187930]
21. Moeller S, Yacoub E, Olman CA, Auerbach E, Strupp J, Harel N, Ugurbil K. Multiband Multislice GE-EPI at 7 Tesla, With 16-Fold Acceleration Using Partial Parallel Imaging With Application to High Spatial and Temporal Whole-Brain FMRI. Magnetic resonance in medicine: official journal of the Society of Magnetic Resonance in Medicine/Society of Magnetic Resonance in Medicine. 2010; 63:1144–1153.
22. Larkman DJ, Hajnal JV, Herlihy AH, Coutts GA, Young IR, Ehnholm G. Use of multicoil arrays for separation of signal from multiple slices simultaneously excited. Journal of Magnetic Resonance Imaging. 2001; 13:313–317. [PubMed: 11169840]
23. Pfeuffer J, Moortele PFvd, Yacoub E, Shmuel A, Adriany G, Andersen P, Merkle H, Garwood M, Ugurbil K, Hu X. Zoomed Functional Imaging in the Human Brain at 7 Tesla with Simultaneous High Spatial and High Temporal Resolution. NeuroImage. 2002; 17:272–286. [PubMed: 12482083]
24. Yushkevich PA, Piven J, Hazlett HC, Smith RG, Ho S, Gee JC, Gerig G. User-guided 3D active contour segmentation of anatomical structures: Significantly improved efficiency and reliability. NeuroImage. 2006; 31:1116–1128. [PubMed: 16545965]
25. Xu G, Pan Q, Bajaj CL. Discrete surface modelling using partial differential equations. Computer Aided Geometric Design. 2006; 23:125–145. [PubMed: 19830268]
26. Dale AM, Fischl B, Sereno MI. Cortical Surface-Based Analysis: I. Segmentation and Surface Reconstruction. NeuroImage. 1999; 9:179–194. [PubMed: 9931268]
27. Khan R, Zhang Q, Darayan S, Dhandapani S, Katyal S, Greene C, Bajaj C, Ress D. Surface-based analysis methods for high-resolution functional magnetic resonance imaging. Graphical Models. 2011; 73:313–322. Computational Modeling in Imaging Sciences. [PubMed: 22125419]
28. Efron, B., Tibshirani, RJ. An introduction to the bootstrap. CRC press; 1994.
29. Efron, B., Efron, B. The jackknife, the bootstrap and other resampling plans. Vol. 38. SIAM; 1982.
30. Efron B. Bootstrap methods: another look at the jackknife. The annals of Statistics. 1979:1–26.
31. Greene CA, Dumoulin SO, Harvey BM, Ress D. Measurement of population receptive fields in human early visual cortex using back-projection tomography. Journal of vision. 2014; 14:17.
32. Katyal S, Greene CA, Ress D. High-resolution functional magnetic resonance imaging methods for human midbrain. J Vis Exp. 2012; 63:e3746.
33. Kruger G, Glover GH. Physiological noise in oxygenation-sensitive magnetic resonance imaging. Magnetic Resonance in Medicine. 2001; 46:631–637. [PubMed: 11590638]
34. Robson MD, Gore JC, Constable RT. Measurement of the point spread function in MRI using constant time imaging. Magnetic Resonance in Medicine. 1997; 38:733–740. [PubMed: 9358447]

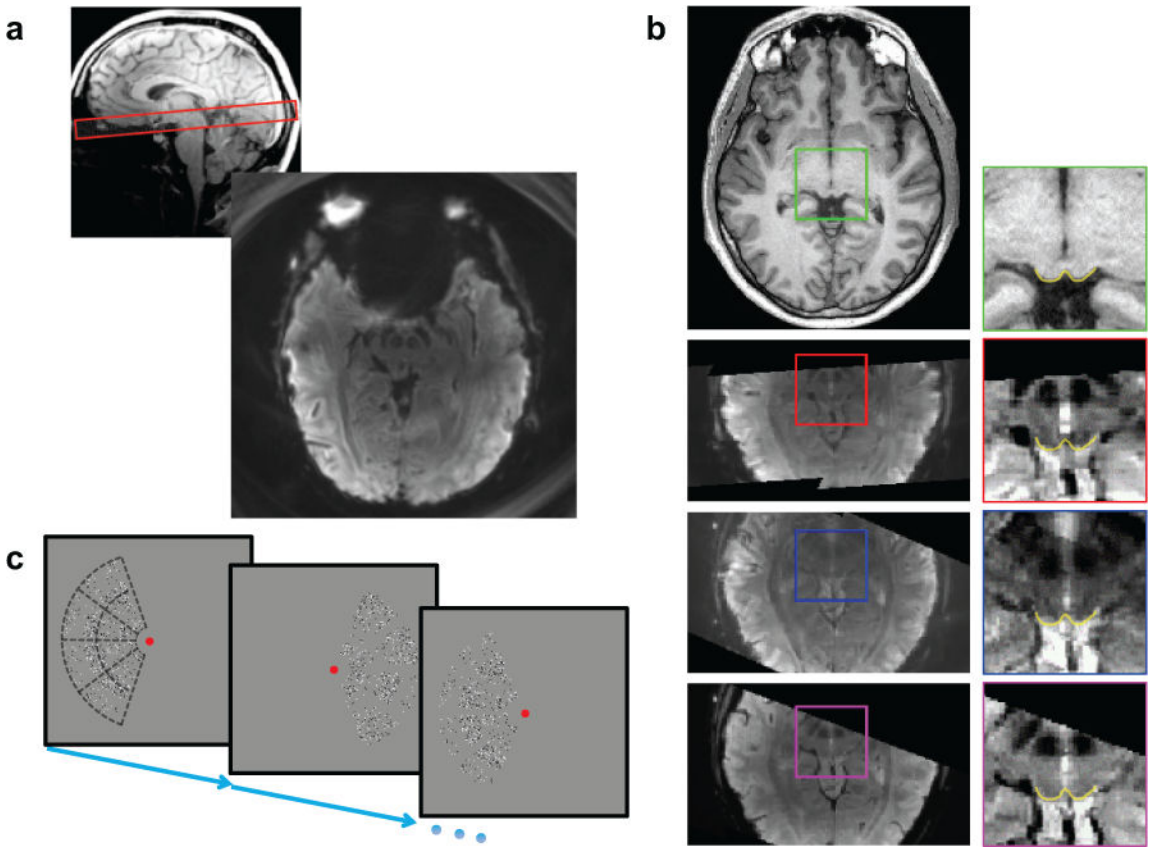

Figure 1.

(a) Typical prescription (top) and acquired functional image (bottom). (b) Axial slice from structural reference volume (1st row), corresponding transformed functional data for spiral-out (2nd row), spiral-in (3rd row) and, EPI (4th row) trajectories. Enlargements on right show SC superficial surface (yellow) obtained from structural volume (green inset), and its close correspondence to contrast boundaries in the functional images (red inset- out; blue- in; magenta- EPI). (c) The lateralized hemi-field moving dot stimulus. Subjects performed a speed-discrimination task among virtual sectors shown as dotted outlines in first image. Stimulus alternated from left to right hemi-field with a 24-s period.

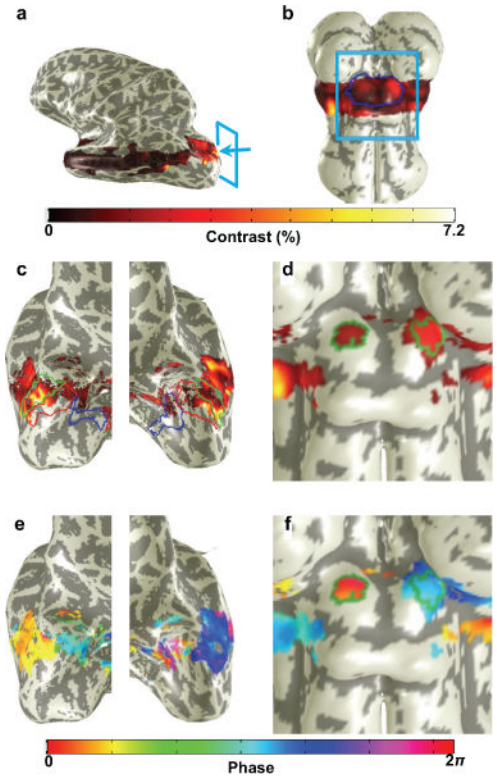

Figure 2.

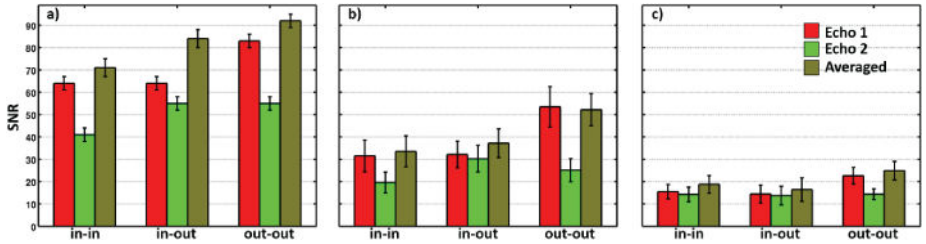

Figure 3.

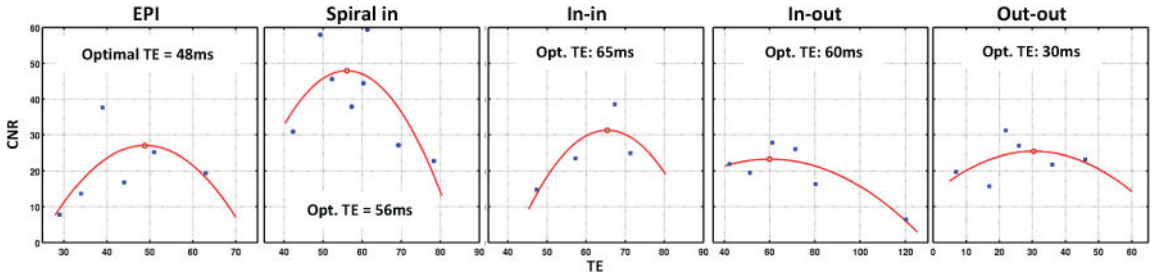

Figure 4.

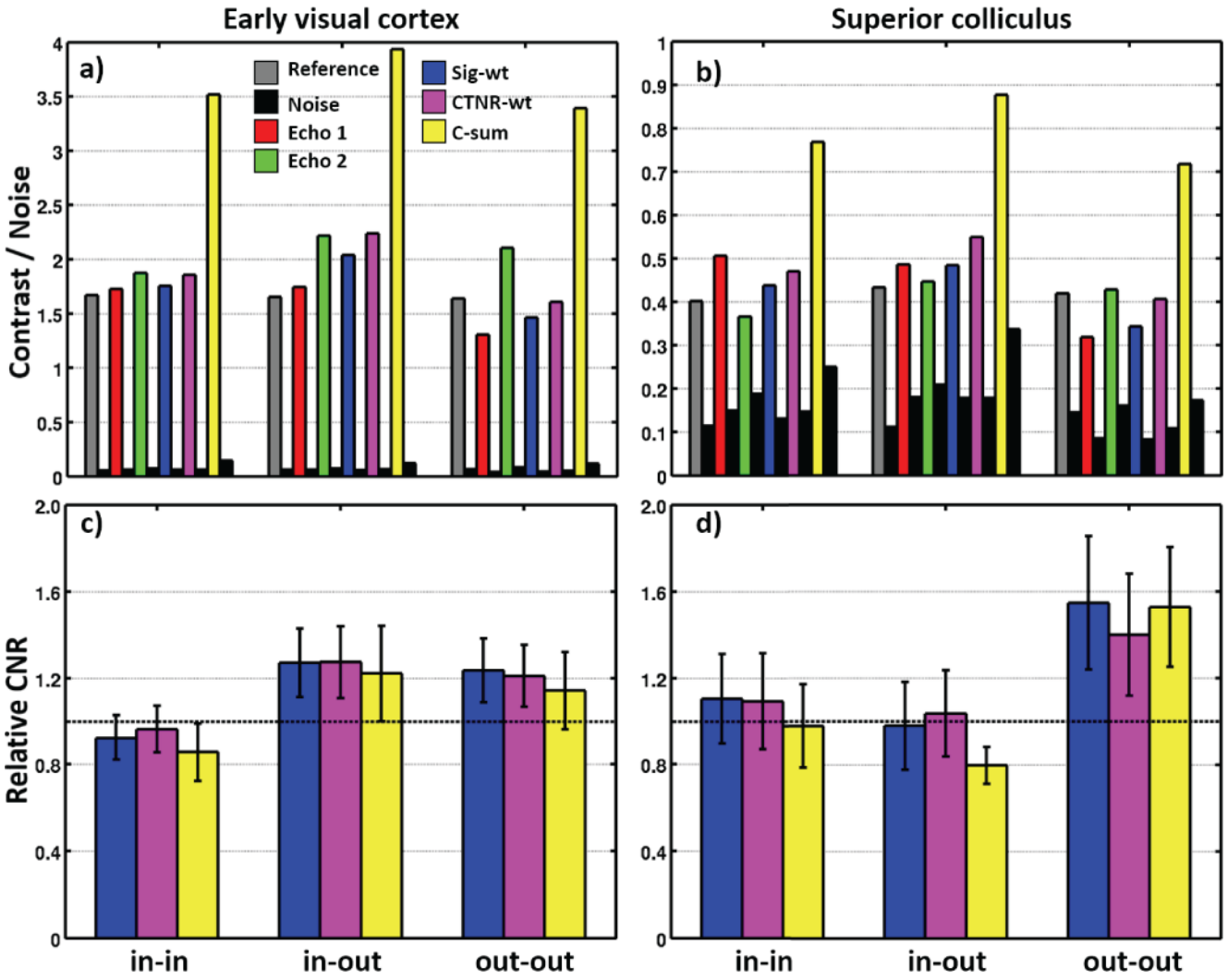

Figure 5.

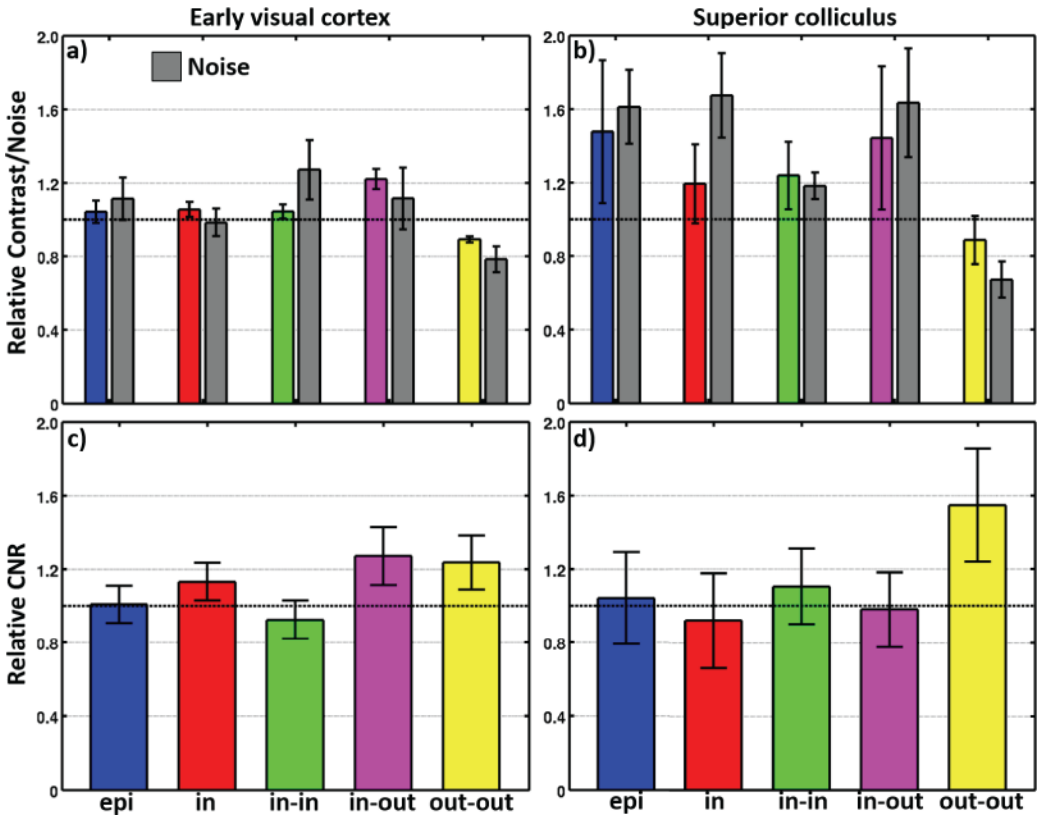

Figure 6.

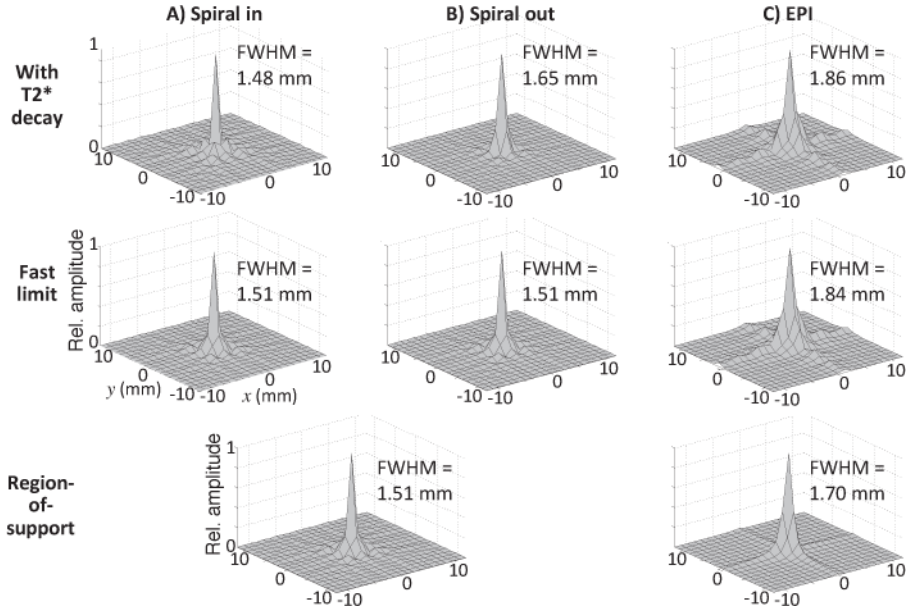

Figure 7.